Poly (caprolactone)-poly (N-isopropyl acrylamide)-Fe₃O₄ Magnetic Nanofibrous Structure with Stimuli Responsive Drug Release

Sanaz Gholami[1], Sheyda Labbaf[1*], Ahmad Kermanpur[1], Arezou Baharlou Houreh[2], Chaojie Luo[3], Mohan Edirisinghe[3], Mohammad-Hossein Nasr Esfahani[2],

[1] Biomaterials Research Group, Department of Materials Engineering, Isfahan University of Technology, Isfahan, 84156-83111, Iran

[2] Department of Cellular Biotechnology, Cell Science Research Center, Royan Institute for Biotechnology, ACECR, Isfahan, Iran

[3] Department of Mechanical Engineering, University College London, Torrington Place WC1E 7JE, London, UK

Corresponding author: s.labbaf@iut.ac.ir

Abstract

Poly (caprolactone; PCL) - poly (N-isopropylacrylamie; PNIPAAm) - Fe₃O₄ fiber, that can be magnetically actuated, is reported. Here, we engineer a structure that can be utilized as a smart carrier for the release of chemotherapeutic drug via magneto-thermal activation, with the aid of magnetic nanoparticles (MNPs). The magnetic measurement of the fibers revealed saturation magnetization values within the range of 1.2-2.2 emu/g. The magnetic PCL-PNIPAAm-Fe₃O₄ scaffold showed a specific loss power value of 4.19 W/g at 20wt% MNPs. A temperature increase of 40 °C led to a 600% swelling after only 3 h. Doxorubicin (DOX) as a model drug, demonstrated a controllable drug release profile. $39\% \pm 0.92$ of the total drug loaded was released after 96 h at 37 °C, while 25% drug release in 3 h at 40 °C was detected. Cytotoxicity results showed no significant difference in cell attachment efficiency between the MNP-loaded fibers and control while the DOX-loaded fibers

effectively inhibited cell proliferation at 24 h matching the drug release profile. The non-cytotoxic effect, coupled with the magneto-thermal property and controlled drug release, renders excellent potential for these fibers to be used as a smart drug-release agent for localized cancer therapy.

Key words: Poly (caprolactone); Poly (N-isopropylacrylamie); Fe_3O_4; magnetic fibrous structure; hyperthermia.

1. Introduction

The most common treatment for cancer is chemotherapy and radiotherapy [1]. However, these therapeutic approaches cause serious side effects to normal cells and the lack of selectivity toward cancer cells is the main drawback [2]. An interesting approach is the utilization of a stimuli-responsive polymeric structure that can respond to an external stimuli such as temperature, light, electrical or magnetic fields [3, 4]. One of the best studied environmentally responsive polymers is the water-soluble thermo-sensitive poly (N-isopropylacrylamide) (PNIPAAm) with a low critical solution temperature (LCST) of 32 ^{o}C [5]. Above LCST, the hydrated polymer shrinks and releases its cargo, making them ideal as a smart thermoresponsive polymer for medical applications [6].

Recently, magnetic nanoparticles (MNPs) have received great attention for cancer therapy applications because of their low toxicity, low cost and easy of preparation [7] . Also, MNPs can be activated by an external alternating magnetic field (AMF) and can act as a heat generating source for hyperthermia applications [8-12]. These heat generating sources can increase the local temperature up to 41-45 $^{\circ}C$ and hence cause tumor cell death [13, 14]. Zhang et al. [15] fabricated a three-dimensional composite membrane of poly(ϵ-caprolactone)-poly (ethylene glycol)- poly(ϵ-caprolactone) containing 10%(w/w) Fe_3O_4 nanoparticles by co-spinning technique and confirmed the non-cytotoxic nature of the resultant structure. In a study by Kim et al. [16], co-polymer of NIPAAm and N-hydroxymethylacrylamide (HMAAm) (poly (NIPAAm-co-HMAAm)) nanofiber was used to encapsulate DOX and MNPs (Fe_3O_4) and maghemite (γ-Fe_2O_3) through electrospinning. In the presence of nanoparticles and doxorubicin (DOX), 70% of human melanoma cells were destroyed in 5 min by applying an AMF. DOX is a well-known chemotherapeutic drug that causes cell death by damaging DNA [17]. Slemming-Adamsen et al. [18] electrospinned *in situ* cross-linked PNIPAAm-gelatin nanofibers with DOX encapsulation and showed that at 40 °C, DOX release caused significant reduction in Hela cell viability. In a different study, a

2

smart injectable thermoresponsive hydrogel formed by alginate-g-PNIPAAm loaded with DOX was synthesized, where a more sustained release of DOX was achieved with a good efficiency for killing the cancer cells [3]. Many studies have proved the application of PNIPAAm nanofibers in the field of controlled drug release due to its thermosensitive characteristics. Nevertheless, due to the poor electrospinnability and biocompatibility of PNIPAAm, blending it with other polymers is suggested [19]. Among synthetic polymers, polycaprolactone (PCL) is commonly used for the fabrication of uniform fibers. In addition, this polymer would enhance the biocompatibility of the polymeric network and can be used in long term drug delivery system due to its low degradation rate [20].

In this study, MNPs and DOX are encapsulated in PCL- PNIPAAm nanofibrous membrane [21] through electrospinning, a simple versatile technique, to resemble the structure of extracellular matrix (ECM) [22, 23] and to simultaneously enable a more efficient cancer therapy approach. Other techniques such as centrifugal spinning and pressurized gyration are also viable in order to mass produce the nano-fibres prepared in this way[24].

2. Materials and methods

2.1 Fe_3O_4 nanoparticle synthesis

MNPs were prepared through co-precipitation method as previously described [21]. All precursors were purchased from Merck, Germany. In brief, 60 mL and 30 mL ferric and ferrous chloride solutions (0.1 M) were prepared separately. Then both solutions were mixed in a three-necked round flask under nitrogen atmosphere. After 15 min, 7mL ammonia solution was added dropwise to the above solution and caused a color transition that showed black magnetite crystals were formed. Finally, MNPs were washed three times with distilled water and ethanol to remove excess ammonia. MNPs were dried at 60 ^oC in vacuum for 5 h.

2.2 PCL-PNIPAAm nanofiber fabrication

Fibers were prepared by using PCL-PNIPAAm solution at a ratio of 1:1. PCL (80000, Sigma-Aldrich Co. USA) was dissolved in a 1:3 mixture of methanol and chloroform (Merck,

Germany). Then, PNIPAAm (40000, Sigma-Aldrich) was dissolved into the mixed solvent. Once the homogenous polymer solution was obtained, electrospinning was carried out in a 1 mL syringe fitted with a metallic needle of 21 gauge. The electrospinning conditions were as follows: a voltage of 11 kV, a needle to collector distance of 110 mm and a flow rate of 1 mL/h.

2.3 Magnetic PCL-PNIPAAm fabrications

For the preparation of magnetic PCL-PNIPAAm solution, 10wt% and 20wt% MNPs were added to the as prepared polymeric solution. MNPs were dispersed in the solution with probe sonication for 5 min. After getting a black solution, it was transferred into the syringe immediately to avoid nanoparticle agglomeration. Electrospinning parameters were as discussed above. During electrospinning, to avoid MNPs agglomeration in the syringe, after time interval of 20min, the solution was transferred to a probe sonicator for homogenization.

2.4 Characterization of PCL-PNIPAAm magnetic fibers

X-ray diffraction (XRD) analysis

To determine the phase structure of nanocomposite fibers, X-ray diffractometer (X'pert Philips) with Cu Kα source radiation (λ=0.154 nm) was used. The samples were scanned at $2\theta=10\text{-}90^{\circ}$, at a voltage of 40 kV and a current of 30 mA. The average diameter of magnetic nanoparticles was calculated according to Scherrer's equation (Eq.1)

$$D= K\lambda /\beta\cos\theta \tag{1}$$

Where D is the average crystallite size, K is the grain shape factor (0.94), λ is X-ray wavelength of Cu Kα radiation (0.154 nm), β is the full width at half-maximum intensity and θ is the Bragg diffraction angle. The most intense peak (311) was chosen to determine the average diameter of MNPs [14].

Scanning electron microscopy (SEM) analysis

The morphologies of the electrospun fibers were investigated using scanning electron microscopy (Philips XL30) operated at 30 kV. SEM samples were gold sputtered and then analyzed. The average fibers diameter was estimated using Image J software by measuring 20 fibers.

Vibrating sample magnetometer (VSM) analysis

Magnetic properties were measured in a vibrating sample magnetometer (VSM) under a maximum applied magnetic field of 12000 Oe at room temperature.

Magnetic heating properties of the scaffolds

Heating properties were carried out by placing 5 mg nanoparticles or fibers in a glass tube containing 1 mL distilled water in the center of a coil of a custom-built magnetic field generator with an efficient field intensity of 6 kA/m at a frequency of v=330 kHz. The SLP value was measured using Eq.2:

$$\mathbf{SLP} = \sum \left| \frac{C_i m_i + A}{m} \right| dT/dt \tag{2}$$

Where C_i is specific heat capacity of magnetite and water and are 650 J/kgK and 4180 J/kgK , respectively, m_i is the mass of magnetite and water, A is water equivalent of glass tube (11.28 J/K), Teflon coating and alcohol thermometer, and m is the mass of magnetic nanofibers in fluid. The term $\dfrac{dT}{dt}$ is the slope of temperature versus time performed by a linear fit to the curve at the initial time interval in the experiment [25]. Eq.3 determines intrinsic loss power, which is produced by the transformation of the energy absorbed by the magnetic nanofibers into heat:

$$ILP=SLP/H^2f \tag{3}$$

Where H is the intensity and f is frequency of the magnetic field that are 6 kA/m and 330 kHz, respectively.

Fourier transform infrared spectrometer (FTIR) analysis

The infrared spectra was recorded in the range 500-4000 cm^{-1} on a Fourier transform infrared spectrometer (FTIR; Model Bomem, MB 100). Electrospun fibers were dried overnight before examination.

Thermogravimetric analysis (TGA)

Thermal stability of the electrospun fibers was carried out by differential scanning calorimetry (DSC)-thermogravimetric (TGA) experiments. TGA-DSC analysis was examined at a heating rate of 10 ^{o}C min^{-1} from 25°C to 500 ^{o}C in air atmosphere.

Hydrophilicity study

The wettability of the scaffolds was evaluated by measuring the water contact angle using a CA-500A analyzer. A 4 µL water droplet in time duration of three seconds was poured on the surface of each sample to measure the angle between the droplet and the scaffold. It should be noted that each droplet was poured in the middle of each sample.

Swelling behavior

The swelling behavior of the PCL-PNIPAAm-DOX electrospun fibers were carried out at 37 ^{o}C (biological body temperature) and 40 ^{o}C (the temperature when exposed to an AMF) in PBS solution. Fibers were weighed and then placed in a shaker incubator (SCI FINETECH Co.). Swollen scaffolds were examined at regular time intervals (1, 2, 3, 24, 48, 72, 96 h),

weighed and then placed in the bath. The percent mass swelling was determined based on the following equation (Eq.4):

$$\text{Swelling (\%)} = \frac{(W_t - W_0)}{W_0} \times 100 \tag{4}$$

Where W_0 and W_t are the initial mass and mass at different time-intervals, respectively. All experiments were carried out for three samples.

2.5 Drug loading and release of DOX

Briefly, 2 wt% of DOX drug was added to PCL-PNIPAAm solution and stirred for 1 h in darkness. Following mixing, electrospinning was carried out according to section 2.2 and the resultant fibers were left in a desiccator overnight. To measure the release of DOX, electrospun fibers were cut into 20×20 mm^2 pieces and immersed in PBS solution. The samples were placed in a shaker incubator at 37 $^{\circ}$C for 1, 2, 3, 24, 48, 72, 96 h and 40 $^{\circ}$C for 1, 2, 3 h. The amount of drug release was analyzed via UV-vis spectrophotometry (Model EU-2800DS). The drug release percentage was calculated according to the following equation (Eq.5):

$$\text{Released drug} = \frac{M_t}{M_{tot}} \times 100 \tag{5}$$

Where M_t is the mass of DOX released at time (t) and M_{tot} is the total mass of DOX on the fibrous mat.

2.6 Cell study

Human osteoblast-like cells (MG63) were obtained from the Pasteur Institute (Iran). Dulbecco's modified eagle's medium-high glucose12800 (DMEM12800), fetal bovine serum (FBS), penicillin, streptomycin, glutamax and trypsin/EDTA solution were obtained from

Gibco (Germany). MG63 cells were cultured in Dulbecco's modified Eagle's medium (DMEM) supplemented with 10% FBS, 100 U/mL penicillin-streptomycin and 1% glutamax at 37 °C in a humidified atmosphere of 5% CO_2. Fibers were sterilized under UV for 40 minutes and washed twice with PBS and put in penicillin/Streptomycin/gentamicin.

Cell attachment

MG-63 osteoblast-like cells were seeded at a density of 30,000 cell/scaffold and incubated for 24 h at 37 °C in a humidified atmosphere of 5% CO_2. At day 1, cells were fixed with 2.5% gluteraldehyde (Sigma, UK) in PBS for 40 minutes at 4 °C. Cells were dehydrated through a series of increasing concentration of graded ethanol (0, 25, 50, 75 and 100%). Samples were sputter coated with gold and viewed using a scanning electron microscope (SEM, type of Philips XL30).

Cell attachment and viability

MTS cytotoxicity/proliferation assay (Invitrogen, UK) was performed according to the manufacturer's protocol. Initially, MG63 cells were cultured at a density of 30,000 cell/scaffold for 4 h to evaluate cell attachment. At days 1, 3 and 6 cell proliferation was studied. At the end of each time point, MTS reagent was added to each well and incubated for 3.5 h at 37 °C after which absorbance was measured at 450 nm using a microplate reader.

Statistical Analysis

Statistical differences were determined by one-way ANOVA, with $p \leq 0.05$ considered significant.

3. Results and discussion

Fig. 1 presents Fe_3O_4 magnetite XRD peaks detected at $2\theta = 30^\circ$, 35°, 43°, 53°, 57° and 63° corresponding to planes (220), (311), (400), (422), (511) and (440), demonstrating a cubic

spinel structure [21]. The crystallite size of MNPs was calculated according to Scherrer's equation (Eq.1) and was found to be 21 nm. The PCL-PNIPAAm XRD pattern (Fig.1) exhibits two defined crystalline peaks at $2\theta = 21$ and 23° suggesting uniform interaction between the polymers [26, 27]. The diffraction peaks at $2\theta = 30^{o}, 35^{o}, 43^{o}$ and 57° reveals the crystalline peaks of MNPs (10 and 20 wt% tested) within the PCPN fibers which are related to planes (220), (311), (400) and (511) [26]. The results also demonstrate that the magnetite peaks intensify with increased concentration of MNPs.
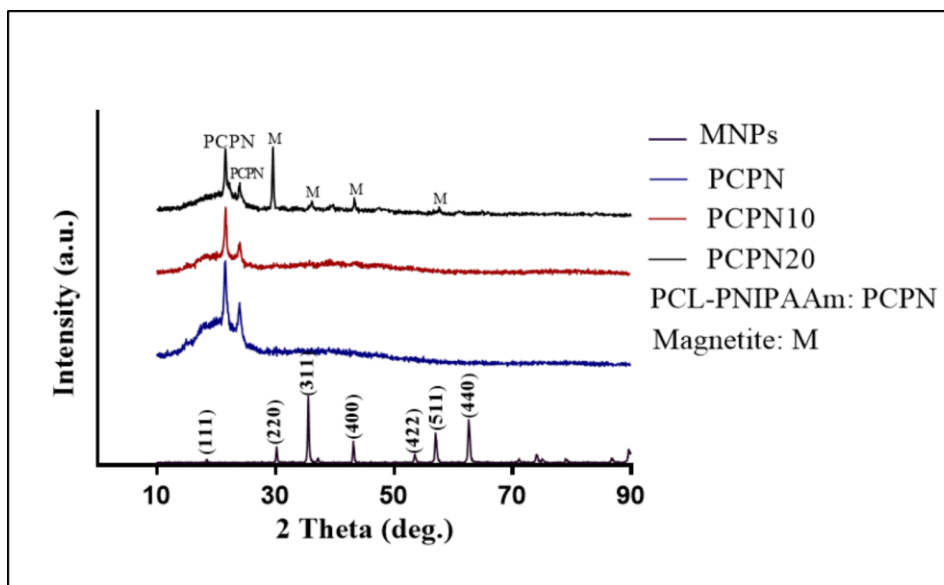
Figure 1: X-ray diffraction pattern for PCL/PNIPAAm and 10 and 20 wt% Fe_3O_4 in PCL/PNIPAAm fibers.

In Fig. 2 SEM images of randomly orientated nanofibers of PCPN without and with MNPs are presented. It is evident that all fibers are in nanoscale and possess a porous structure. Flow rate of the polymer solution, the distance between syringe tip to the collector and applied voltage are the parameters that affect the morphology and diameter of electrospun fibers. Since these parameters were constant for PCPN, PCPN10 and PCPN 20, it can be concluded that the MNP concentration plays the important role in the fiber morphology[28]. As can be seen the PCPN fibers appear to have a bead-free smooth surface with an average diameter of 569±195 nm. During electrospining, the MNPs could either be incorporated within the fibers or appear on the surface of the magnetic scaffolds giving it a unique surface

texture/topography. The diameter of PCPN10 and PCPN20 were estimated to be 294±80 nm and 291±79 nm, respectively. Previous studies have shown that MNP concentration can influence fiber diameter as a result of changes in viscosity and electrical conductivity of polymer solution [29]. Under a higher voltage, the spinning solution can be stretched into thinner fibers owing to a stronger electric field potential acting on the spinning dope [15].
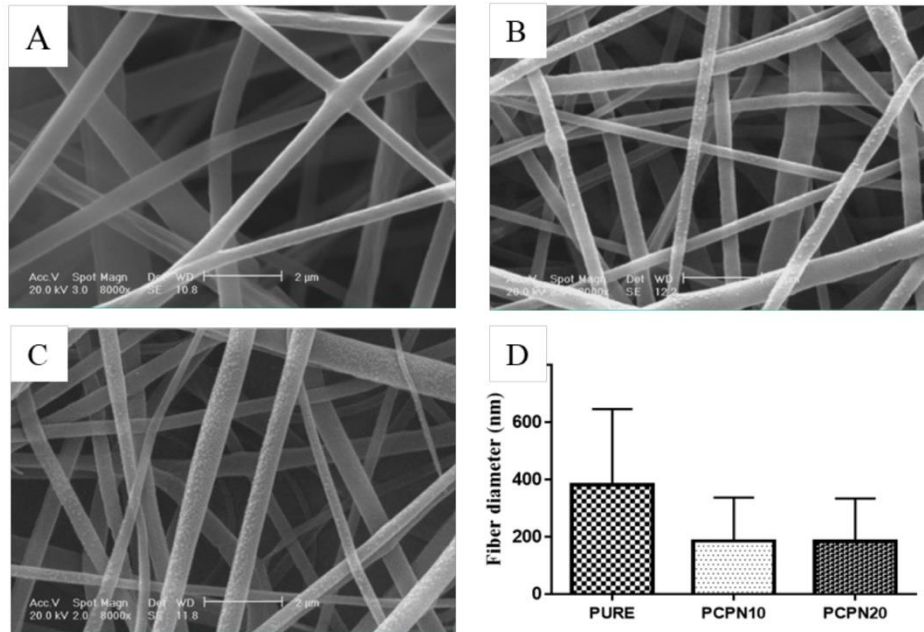

Figure 2: SEM images of electrospun PCL/PNIPAAm (PCPN) fibers with A) 0 wt%, B) 10 wt%, C) 20 wt% MNPs and D) the corresponding histogram size distribution of the fibers.

Fig. 3 (A and B) shows M-H curves of Fe_3O_4 nanoparticles and magnetic nanofiber with different concentration of Fe_3O_4. In Fig. 3A, the saturation magnetization (M_s) of MNPs is 81.2 emu/g with the appearance of a hysteresis loop in magnetization curve. This observation is related to increased particle size of Fe_3O_4 which is significantly above the critical size (20 nm) required for a superparamagnetic behavior [30]. Therefore, a transition from a single domain, typical of superparamagnetic material, to multi-domain for paramagnetic Fe_3O_4 nanoparticles is detected. In a multi-domain structure, some domains may retain their magnetic properties when the external AMF is removed, so by reaching zero point, there is small coercivity (H_c) and remanence in the as-synthesized nanoparticles. This is a typical

trend for MNPs above 20 nm in size owed to their increased magnetic anisotropy energy resulting in detectable coercivity in the magnetic curves [31, 32].

Furthermore, the saturation magnetization (M_s), remnant magnetization (M_r) and coercive field (H_c) for PCPN10 are 1.29 emu/g, 0.2 emu/g, 120 Oe and for PCPN20 are 2.21 emu/g, 0.35 emu/g, and 120 Oe. In a study by Kim et al. [33], a magnetic nanocomposite scaffold made of PCL and MNPs showed a magnetization value of 1.6 and 3.1 emu/g for 5% and 10% MNP content, respectively. In another study, PCL scaffold containing 8 wt% MNPs showed a saturation magnetization of 6.1±0.3 Am^2 at 300 K [34]. In another study the value of M_s for a magnetic nanocomposites scaffold was in the range 0.1-0.3 emu/g that was due to the small amount of MNPs, which was much smaller than the PCL matrix mass [35].

To evaluate the efficiency of the magnetic nanofiber for therapeutic hyperthermia, magnetic heating properties were investigated. According to Fig. 3C, under an applied field strength of 6 kA/m at a frequency of 330 kHz, the solution temperature for MNP increased to 61 °C within 10 min. As shown, the temperature of PCPN10 increased from 32 to 37 °C in AMF while PCPN20 showed a temperature increase of 40 °C in the same period of time. The difference between the increased temperature of MNPs and MNPs loaded fibers is due to MNPs that are influenced by electrospun fibers and cannot be fully activated under an external AMF.

The SLP values for all samples are listed in Table 1. The intrinsic loss power (ILP) parameter was calculated to compare heating efficiency. With increase in the maximum temperature of the samples, the ILP values also increased (Table 1). In agreement with the magnetic results, by increasing the magnetic particles within the polymeric structure, the magnetically induced heating property of the scaffold increases [13, 35]. PCL-PNIPAAm- 20 wt% MNPs scaffolds possessed a better thermal efficiency under an external magnetic field. Zhang et al.[13] fabricated PCL-mesoporous bioactive glass (MBG) enriched MNPs. The SLP studies

demonstrated that the solution temperature of the scaffold with 15% MNPs increased from 20 to 43 °C within 2 min at the AC frequency of 409 kHz.
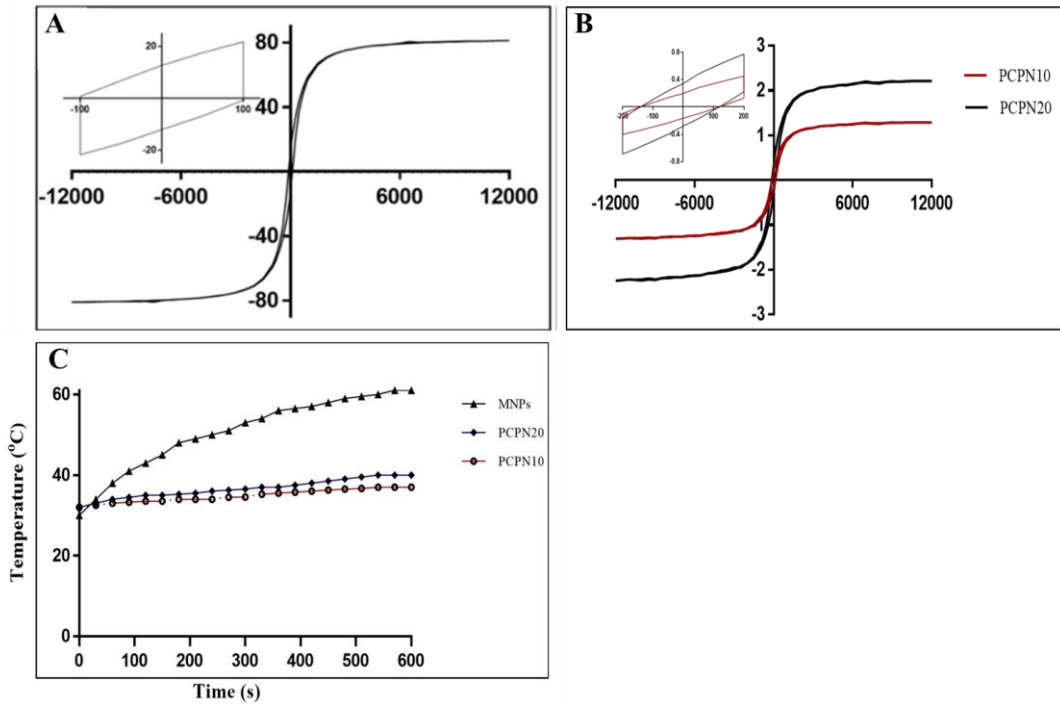
Figure 3: Vibrating sample magnetometer (VSM) of A) MNPs and B) magnetic PCL-PNIPAAm fibers C) Temperature versus time for magnetic nanoparticles and magnetic PCL/PNIPAAm fibers under an alternating magnetic field of 330 kHz.

Table 1: The SLP and ILP values for MNPs and electrospun fibers.

Samples	dT/dt (°C/s)	SLP (W/g)	ILP (nHm^2/kg)	Maximum temperature after 10 min (°C)
MNPs	0.13	15.36	1.29	61
PCPN10	0.02	2.36	0.20	37
PCPN20	0.03	3.54	0.30	40

FTIR spectra of PCPN10 and PCPN20 are illustrated in Fig. 4. The band at 1721 cm^{-1} represents the stretching of (C=O) [36]. Peaks at 1047 cm^{-1} and 1180 cm^{-1} are related to the (C-O) band in PCL. The peaks at 1238 cm^{-1}, 1293 cm^{-1} and 1470 cm^{-1} are associated with (C-

O-C), (C-C) and (C-H) banding in PCL, respectively [36]. The asymmetric and symmetric CH$_2$ banding at 2946 cm^{-1} and 2865 cm^{-1} are also related to PCL [37]. The characteristic bands of PNIPAAm at 1387 cm^{-1}, 1653 cm^{-1}and 3300 cm^{-1} are corresponding to CH$_2$, NH$_2$ and NH-OH groups, respectively [38]. Peaks at 3448 cm^{-1} indicate Fe-OH bond [39] and at 585 cm^{-1} the absorption bands of Fe-O in magnetite is detected [40], which intensifies at higher concentration of MNP in fiber.
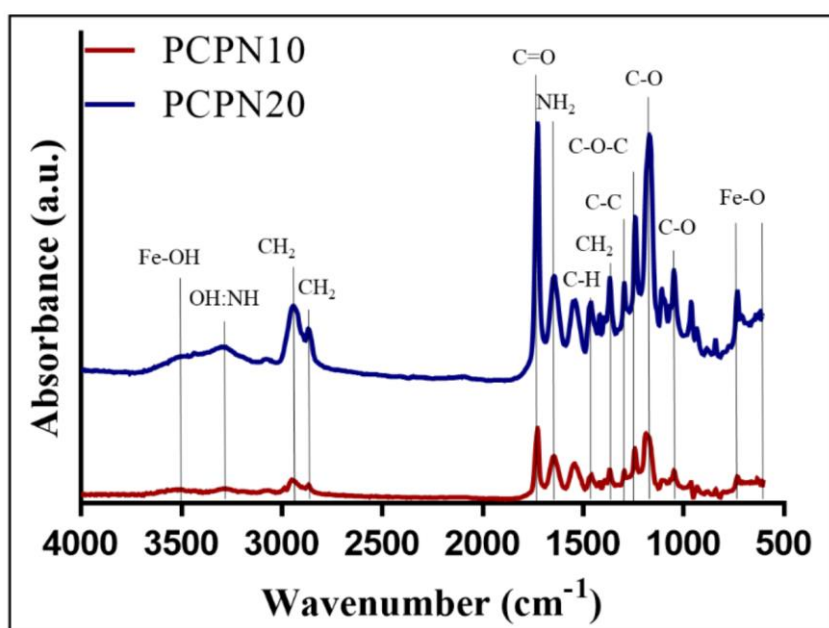

Figure 4: FTIR spectra of PCL/PNIPAAm (PCPN) fibers with 10 wt% and 20 wt%MNPs.

The thermal stability of the prepared scaffolds was evaluated from room temperature to 500 °C using TGA, which shows single stage decomposition for electrospun fibers. To evaluate the phase transition temperature of the scaffolds, DSC was utilized [41]. As can be seen in Fig. 5, an increase in mass of about 10% from 25-332 °C for all three samples is detected due to surface oxidation. An endothermic peak at 58 °C can be seen (which is more obvious in Fig. 5 A and C) that is related to the melting point of PCL [42]. An endothermic peak at 100 °C from the DSC is due to water molecules evaporation. The main weight loss of 92% at 356

13

°C is due to the thermal destruction process of PNIPAAm chains [43]. The DSC curves also exhibit the decomposition of PNIPAAm at an exothermic peak at 356 °C that proves the high thermal stability of this polymer. The mass loss observed in temperature range of 400 °C may be due to the removal of oxygen functionalities [25]. The thermal decomposition of PCL is at 400 °C [33]. A small difference in the endo and exothermic temperature for the three samples could be due to the presence of MNPs. The incorporation of MNPs does not affect the weight loss, hence, the main weight changes are due to PNIPAAm and PCL degradation. Based on the data analysis, in Fig 5A about 8.5 % fibers remained at 500°C, while in Fig 5B and C the residual weight was 17.5% and 26%, respectively. By reducing the amount of residual polymer from the MNPs, the mass fraction of MNPs was calculated to be about 9% and 17.5% in Fig 5B and 5C, respectively, that is almost near the amount of MNPs loaded into electrospun fibers.
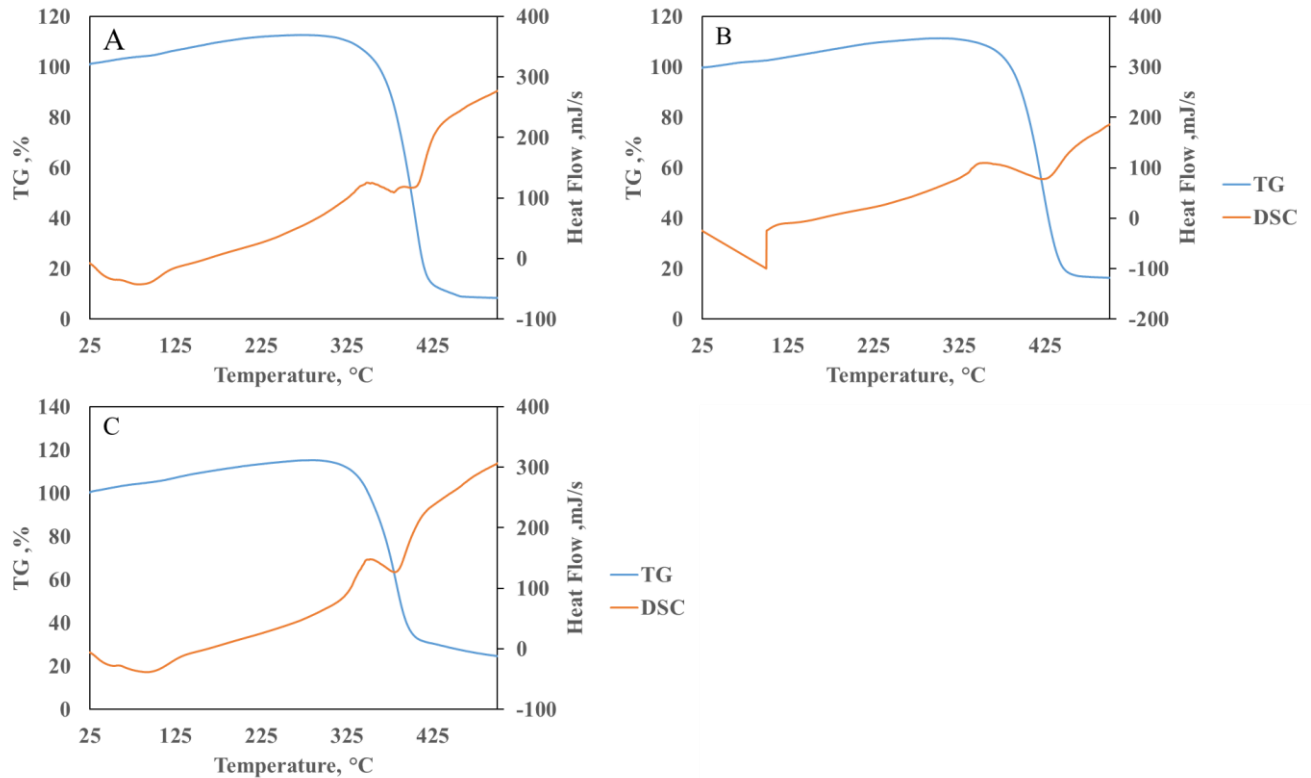

14

Figure 5: Thermogravimetry (TG) and differential scanning calorimetry (DSC) for PCL-PNIPAAm containing A) 0 wt%, B) 10 wt% and C) 20 wt% MNPs.

The hydrophilic nature of the fibers plays an important role as a regulator of protein and cell adhesion [44]. The as-prepared PCL-PNIPAAm with and without MNPs showed a high degree of hydrophilicity (Fig. 6) at room temperature (below the LCST temperature of PNIPAAm). In PCL-PNIPAAm fiber, due to the presence of C=O and N-H groups which interact with water molecules, the scaffold is hydrophilic (a water contact angle of 36.9°) [45]. In PCL-PNIPAAm containing 10 and 20 wt% MNPs, the nanofiber turned more hydrophilic (contact angle from 25.6° to 14.2°), probably owing to the existence of hydroxyl groups (OH groups) on the surface of MNPs [33].
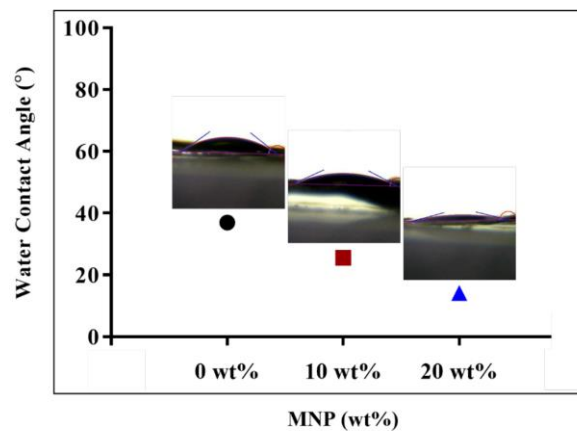

Figure 6: Contact angle measurements for PCL-PNIPAAm contain A) 0wt%, B) 10 wt% and C) 20 wt% MNPs.

In this study, PNIPAAm was chosen as a thermo-responsive polymer to respond to the changes in temperature in an AMF due to the presence of MNPs. Drug release rate can be controlled by the degree of swelling of the electrospun fibers in water. For this purpose, the

15

swelling ratio at temperatures of 37 and 40 °C is investigated. PNIPAAm swelling and deswelling kinetics relies on the sample surface area and chemical composition [46]. Below the LCST, due to the strong hydrophilic property of the amide group, strong water absorption in the PNIPAAm chain segment is achieved [47]. Above the LCST the PNIPAAm chain compacts and become dehydrated[5, 46]. Hence, due to the presence of hydrophilic group (amide groups) of PNIPAAm an increase in swelling has been observed at 37 °C and 40°C. According to Fig. 7A, a large network expansion, due to the presence of hydrophilic groups (for example CONH), has led to a high water absorption. As can be seen, the degree of swelling increased to 700% after 96 h, due to water diffusion into the polymeric chains with time. In the current study, the drug release could be regulated by the degree of fiber swelling in aqueous media that can lead to opening of nanofibrous pores and facilitate the diffusion of loaded drugs. The rate and amount of drug release from the polymeric network depend on the amount of water penetration [48]. At a high temperature, as described above, an opening of the PNIPAAm structure facilitates the diffusion of water into the polymeric chains [49]. At 40 °C, 600% swelling in the first 3 h is detected, due to increased mobility of polymeric chains and higher water diffusion [50]. The release profile of DOX for PCL-PNIPAAm fibers at 37 °C was monitored for 96 h. According to Fig. 7C, a burst release in the first few hours, followed by a sustained release thereafter is evident. In the first stage, the presence of DOX molecules attached on the surface of the fiber causes a burst release (34% ± 0.59) after 24 h. In the second stage, the release rate is relatively constant and after 96 h, 40% ± 0.92 of the total drug loaded is released. The sustained drug release in the second stage is due to drug molecules that are probably bounded to the polymer chains [13]. This process is diffusion controlled and as it can be seen, diffusion is time-dependent and slow. Another reason for the steady release could be the desorption and dissolution process of DOX molecules to the solution [51]. Thus a controllable release profile is seen. The first rapid release could inhibit

16

the proliferation of the tumor cells and the second sustained release helps to avoid repeated administration of the drugs and also the side effects of using multi-chemotherapeutic drugs. The overall low release profile could be due to the stability of the polymeric network up to 96 h [52] and possible entrapment of the remaining drug into the polymeric matrix [53]. Also the low degradation rate of PCL network prolongs the delivery of chemotherapeutic drug [54]. Bo Li et al. [55] observed similar results for DOX-loaded polymeric nanoparticles. This controllable drug release reduce the adverse side effect of DOX to the surrounding tissues [56]. Nevertheless, at 40 °C (Fig. 7D), the DOX release rate is faster due to an increase in swelling, more mobility of the polymeric network and drug molecules. The fiber degradation, through the hydrolysis of ester bonds in PCL [57, 58], leads to more drug release in 3 h. We suggest that some hydrophobic groups in PNIPAAm above the LCST can led to faster drug release at 40ºC. Also, 25% ± 0.55 of the total drug loaded was released at the elevated temperature.
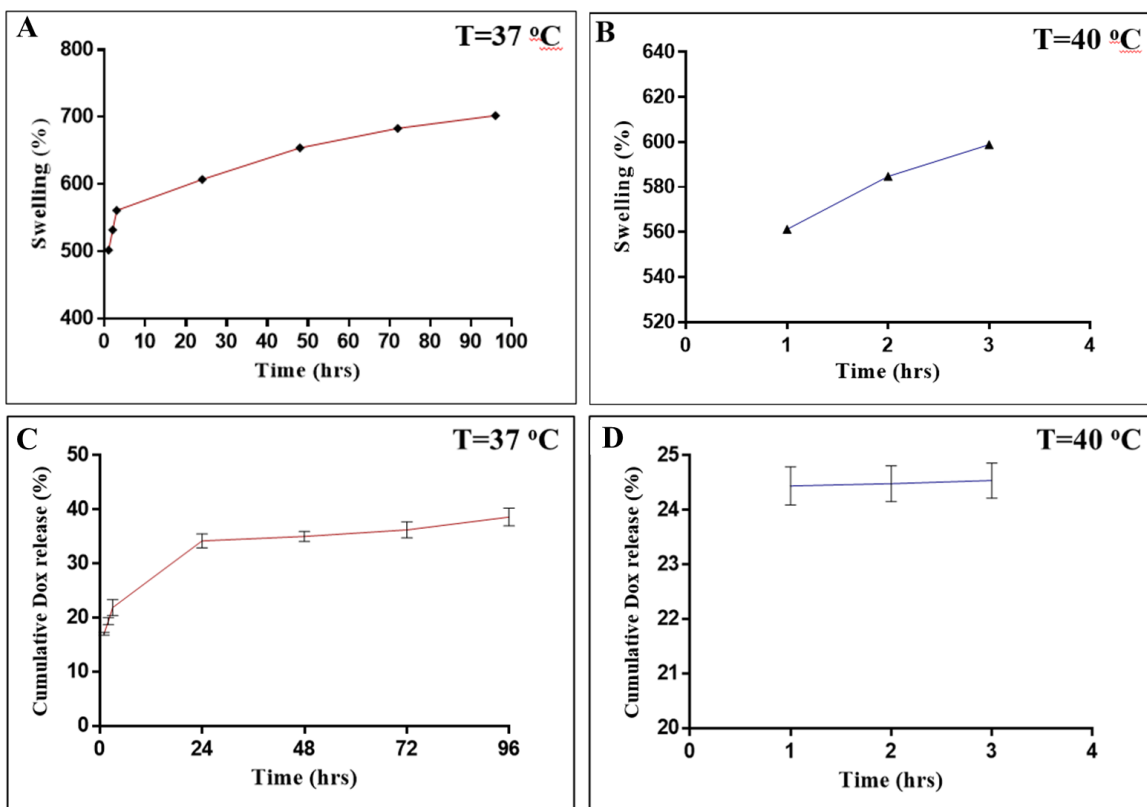
For biological evaluations, MG63 osteoblast-like cell line was utilized. SEM (Fig. 8) clearly demonstrates cell attachment and spreading on fibers with no significant differences between the groups. Cells appear to have maintained their integrity after 24 h culture. As shown in Fig. 9, at day 1, no significant levels of cytotoxicity are detected, except for DOX containing fibers.
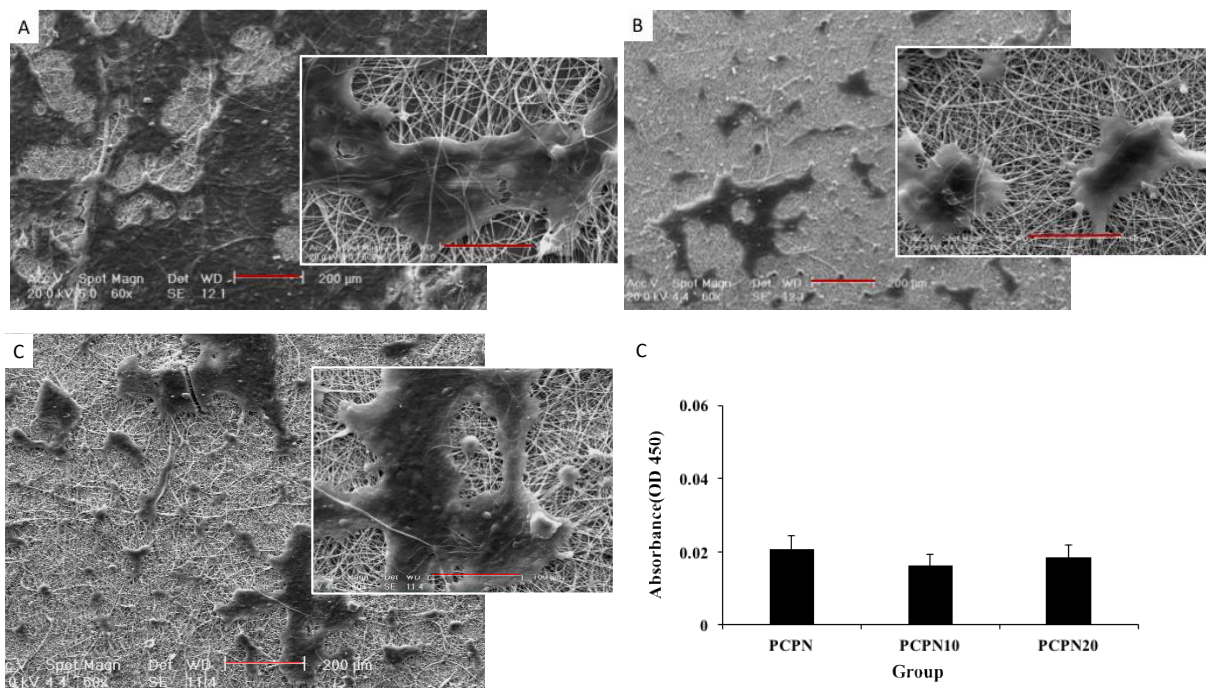

Figure 8: A-C) SEM micrographs of MG63 attachment on control, 10 and 20 wt% Fe_3O_4 fibrous scaffolds following 24 h and D) cell attachment after 4 h post seeding. (SEM scale bar 200 µm and inset 100 µm).

The drug loaded fibers clearly demonstrate a significant level of cell death following 24 h, confirming the efficiency of drug delivery system. This is in good agreement with Fig. 7, which shows 34% drug release following 24 h. In the following days, PCPN control, 10 and 20 wt% MNPs do not appear to have influenced cell growth pattern; however, the cell

proliferation rate is significantly lower than PCPN only. As expected, due to drug release, the cell proliferation rate of DOX containing fibers is significantly lower than the control.

The development of personalized anticancer therapies makes it worthwhile to develop new medical technologies to enable point of care delivery of smart drug release agents such as the fibers reported here. A portable delivery approach would allow wider patient access to advanced nano-medicine which is currently only available in a few select hospitals around the world. Future work will employ portable medical devices to explore the potential to produce and deliver the functionalized fibers for point of care treatment [59, 60].
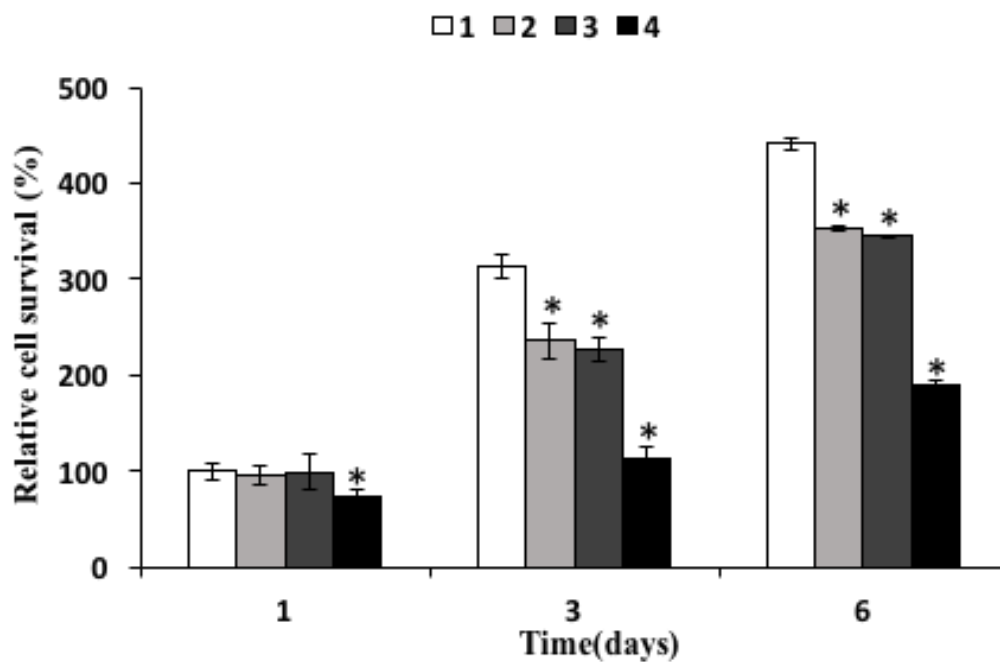

Figure 9: MTS cell viability assay following 1, 3 and 6 days in culture. (*) indicates the statistical significant difference (*p < 0.05 relative to control at the same time point).

Conclusions

A temperature-sensitive magnetic PCL-PNIPAAm scaffold with 10 and 20 wt% MNPs is created through the electrospinning technique. The PCL-PNIPAAm-MNP structure demonstrated a paramagnetic behavior in an AMF. The water contact angle measurements proved the wettability of the electrospun fibers. Swelling studies showed that PCL-PNIPAAm fibers possess higher rate of swelling percentage at an elevated temperature. The release of DOX at pH 7.4 was slow and controllable with about 39% ± 0.92 of the total drug released within 96 h. A faster initial drug release in 3 h at 40 °C was observed as a result of enhanced mobility of polymeric chains at higher temperature. The biological behavior of the electrospun fibers was assessed using MG63 cell lines to evaluate cell attachment and spreading on fibers. Cell attachment efficiency was found not affected by the incorporation of MNPs, while the DOX nanofibers inhibited cell proliferation at 24 h, which matched the DOX drug release profile from the fibers. Future work will employ portable devices for point of need manufacturing of the functional fibers.

Conflict of Interests

The authors confirm no conflict of interest.

References - THIS NEEDS A POLISH UP, THE JOURNAL NAME MUST HAVE CAPITAL LETTERS STARTING EACH WORD…, e.g. ACS Applied Materials & Interfaces, so many corrections, please you do

[1]Beik J, Abed Z, Ghoreishi FS, Hosseini-Nami S, Mehrzadi S, Shakeri-Zadeh A, et al. Nanotechnology in hyperthermia cancer therapy: From fundamental principles to advanced applications. Journal of Controlled Release 2016;235:205-21.

[2]Norouzi M, Nazari B, Miller D. Electrospun-based systems in cancer therapy. Electrospun Materials for Tissue Engineering and Biomedical Applications 2017:337-56.

[3]Liu M, Song X, Wen Y, Zhu J-L, Li J. Injectable thermoresponsive hydrogel formed by alginate-g-poly (N-isopropylacrylamide) that releases doxorubicin-encapsulated micelles as a smart drug delivery system. ACS applied materials & interfaces 2017;9(41):35673-82.

[4]Bawa P, Pillay V, Choonara YE, Du Toit LC. Stimuli-responsive polymers and their applications in drug delivery. Biomedical materials 2009;4(2):022001.

[5]Allen AC, Barone E, Cody O, Crosby K, Suggs LJ, Zoldan J. Electrospun poly (N-isopropyl acrylamide)/poly (caprolactone) fibers for the generation of anisotropic cell sheets. Biomaterials science 2017.69-1661:(8)5;

[6]Cicotte KN, Reed JA, Nguyen PAH, De Lora JA, Hedberg-Dirk EL, Canavan HE. Optimization of electrospun poly (N-isopropyl acrylamide) mats for the rapid reversible adhesion of mammalian cells. Biointerphases 2017;12(2):02C417.

[7]Liu B, Zhang X, Li C, He F, Chen Y, Huang S, et al. Magnetically targeted delivery of DOX loaded Cu 9 S 5@ mSiO 2@ Fe 3 O 4-PEG nanocomposites for combined MR imaging and chemo/photothermal synergistic therapy. Nanoscale 2016;8(25):12560-69.

[8]Rezaei B, Kermanpur A, Labbaf S. Effect of Mn addition on the structural and magnetic properties of Zn-ferrite nanoparticles. Journal of Magnetism and Magnetic Materials 2019;481:16-24.

[9]Souza Jr F, Ferreira A, Varela A, Oliveira G, Machado F, Pereira E, et al. Methodology for determination of magnetic force of polymeric nanocomposites. Polymer Testing 2013;32(8):1466-71.

[10]Sionkowska A, Grabska S. Preparation and characterization of 3D collagen materials with magnetic properties. Polymer Testing 2017;62:382-91.

[11]Vangijzegem T, Stanicki D, Laurent S. Magnetic iron oxide nanoparticles for drug delivery: applications and characteristics. Expert opinion on drug delivery 2019;16(1):69-78.

[12]Feng W, Han X, Wang R, Gao X, Hu P, Yue W, et al. Nanocatalysts-Augmented and Photothermal-Enhanced Tumor-Specific Sequential Nanocatalytic Therapy in Both NIR-I and NIR-II Biowindows. Advanced Materials 2019;31(5):1805919.

[13]Zhang J, Zhao S, Zhu M, Zhu Y, Zhang Y, Liu Z, et al. 3D-printed magnetic Fe_3O_4/MBG/PCL composite scaffolds with multifunctionality of bone regeneration, local anticancer drug delivery and hyperthermia. Journal of Materials Chemistry B 2014;2(43):7583-95.

[14]Singh RK, Patel KD, Lee JH, Lee E-J, Kim J-H, Kim T-H, et al. Potential of magnetic nanofiber scaffolds with mechanical and biological properties applicable for bone regeneration. PloS one 2014;9(4):e91584.

[15]Zhang H, Xia J, Pang X, Zhao M, Wang B, Yang L, et al. Magnetic nanoparticle-loaded electrospun polymeric nanofibers for tissue engineering. Materials Science and Engineering: C 2017;73:537-43.

[16]Kim YJ, Ebara M, Aoyagi T. A smart hyperthermia nanofiber with switchable drug release for inducing cancer apoptosis. Advanced Functional Materials 2013;23(46):5753-61.

[17]El Gohary MI, El Hady BMA ,Al Saeed AA, Tolba E, El Rashedi AM, Saleh S. Electrospinning of doxorubicin loaded silica/poly (ε-caprolactone) hybrid fiber mats for sustained drug release. Advances in Natural Sciences: Nanoscience and Nanotechnology 2018;9(2):025002.

[18]Slemming-Adamsen P, Song J, Dong M, Besenbacher F, Chen M. In Situ Cross-Linked PNIPAM/Gelatin Nanofibers for Thermo-Responsive Drug Release. Macromolecular Materials and Engineering 2015;300(12):1226-31.

[19]Lin X, Tang D, Gu S, Du H, Jiang E. Electrospun poly (N-isopropylacrylamide)/poly (caprolactone)-based polyurethane nanofibers as drug carriers and temperature-controlled release. New Journal of Chemistry 2013;37(8):2433-39.

[20]Simões MCR, Cragg SM, Barbu E, De Sousa FB. The potential of electrospun poly (methyl methacrylate)/polycaprolactone core–sheath fibers for drug delivery applications. Journal of materials science 2019;54(7):5712-25.

[21]Montaseri H, Alipour S, Vakilinezhad MA. Development, evaluation and optimization of superparamagnetite nanoparticles prepared by co-precipitation method. Research in pharmaceutical sciences 2017;12(4):274.

[22]Mortimer CJ, Wright CJ. The fabrication of iron oxide nanoparticle-nanofiber composites by electrospinning and their applications in tissue engineering. Biotechnology journal 2017;12(7):1600693.

[23]Bose S, Roy M, Bandyopadhyay A. Recent advances in bone tissue engineering scaffolds. Trends in biotechnology 2012;30(10):546-54.

[24]Alenezi H, Cam ME, Edirisinghe M. Experimental and theoretical investigation of the fluid behavior during polymeric fiber formation with and without pressure. Applied Physics Reviews 2019;6(4):041401.

[25]Linh P, Phuc N, Hong L, Uyen L, Chien N, Nam P, et al. Dextran coated magnetite high susceptibility nanoparticles for hyperthermia applications. Journal of Magnetism and Magnetic Materials 2018;460:128-36.

[26]Yun H-M, Ahn S-J, Park K-R, Kim M-J, Kim J-J, Jin G-Z, et al. Magnetic nanocomposite scaffolds combined with static magnetic field in the stimulation of osteoblastic differentiation and bone formation. Biomaterials 2016;85:88-98.

[27]Duan Z, Zhang L, Wang H, Han B, Liu B, Kim I. Synthesis of poly (N-isopropylacrylamide)-b-poly (ε-caprolactone) and its inclusion compound of β-cyclodextrin. Reactive and Functional Polymers 2014;82:47.51-

[28]Demir D, Güreş D, Tecim T, Genç R, Bölgen N. Magnetic nanoparticle-loaded electrospun poly (ε-caprolactone) nanofibers for drug delivery applications. Applied Nanoscience 2018;8(6):1461-69.

[29]Kumar M, Unruh D, Sindelar R, Renz F. Preparation of magnetic polylactic acid fiber mats by electrospinning. Nano Hybrids and Composites; 2017: Trans Tech Publ; 2017. p. 39-47.

[30]Mojica Pisciotti ML, Lima Jr E, Vasquez Mansilla M, Tognoli V, Troiani HE, Pasa A, et al. In vitro and in vivo experiments with iron oxide nanoparticles functionalized with DEXTRAN or polyethylene glycol for medical applications: magnetic targeting. Journal of Biomedical Materials Research Part B: Applied Biomaterials 2014;102(4):860-68.

[31]Daňková J, Buzgo M, Vejpravová J, Kubíčková S, Sovková V, Vysloužilová L, et al. Highly efficient mesenchymal stem cell proliferation on poly-ε-caprolactone nanofibers with embedded magnetic nanoparticles. International journal of nanomedicine 2015;10:7307.

[32]Zargar T, Kermanpur A. Effects of hydrothermal process parameters on the physical, magnetic and thermal properties of Zn0. 3Fe2. 7O4 nanoparticles for magnetic hyperthermia applications. Ceramics International 2017;43(7):5794-804.

[33]Kim J-J, Singh RK, Seo S-J, Kim T-H, Kim J-H, Lee E-J, et al. Magnetic scaffolds of polycaprolactone with functionalized magnetite nanoparticles: physicochemical, mechanical, and biological properties effective for bone regeneration. RSC Advances 2014;4(33):17325-36.

[34]Daňková J, Buzgo M, Vejpravova J ,Kubíčková S, Sovková V, Vysloužilová L, et al. Highly efficient mesenchymal stem cell proliferation on poly-ε-caprolactone nanofibers with embedded magnetic nanoparticles. International journal of nanomedicine 2015;10:7307.

[35]Bañobre-López M, Pineiro-Redondo Y, De Santis R, Gloria A, Ambrosio L, Tampieri A, et al. Poly (caprolactone) based magnetic scaffolds for bone tissue engineering. Journal of applied physics 2011;109(7):07B313.

[36]Lepry WC, Smith S, Liverani L, Boccaccini AR, Nazhat SN. Acellular bioactivity of sol-gel derived borate glass-polycaprolactone electrospun scaffolds. Biomedical glasses 2016;2.(1)

[37]Yan X, Duan X-P, Yu S-X, Li Y-M, Lv X, Li J-T, et al. Portable melt electrospinning apparatus without an extra electricity supply. RSC Advances 2017;7(53):33132-36.

[38]Zhang J, Peppas NA. Molecular interactions in poly (methacrylic acid)/poly (N-isopropyl acrylamide) interpenetrating polymer networks. Journal of applied polymer science 2001;82(5):1077-82.

[39]Javidparvar A, Ramezanzadeh B, Ghasemi E. The effect of surface morphology and treatment of Fe3O4 nanoparticles on the corrosion resistance of epoxy coating. Journal of The Taiwan Institute Of Chemical Engineers 2016;61:356-66.

[40]Shan D, Shi Y, Duan S, Wei Y, Cai Q, Yang X. Electrospun magnetic poly (L-lactide)(PLLA) nanofibers by incorporating PLLA-stabilized Fe3O4 nanoparticles. Materials Science and Engineering: C 2013;33(6):3498-505.

[41]Guo X, Du Z, Song M, Qiu L, Shen Y, Yang Y, et al. Grafting thermosensitive PNIPAM onto the surface of carbon spheres. Applied Surface Science 2014;321:116-25.

[42]Heydari Z, Mohebbi-Kalhori D, Afarani MS. Engineered electrospun polycaprolactone (PCL)/octacalcium phosphate (OCP) scaffold for bone tissue engineering. Materials Science and Engineering: C 2017;81:127-32.

[43]Purushotham S, Ramanujan R. Thermoresponsive magnetic composite nanomaterials for multimodal cancer therapy. Acta biomaterialia 2010;6(2):502-10.

[44]Huang A, Jiang Y, Napiwocki B, Mi H, Peng X, Turng L-S. Fabrication of poly (ε-caprolactone) tissue engineering scaffolds with fibrillated and interconnected pores utilizing microcellular injection molding and polymer leaching. RSC Advances 2017;7(69):43432-44.

[45]Chen W, He H, Zhu H, Cheng M, Li Y, Wang S. Thermo-responsive cellulose-based material with switchable wettability for controllable oil/water separation. Polymers 2018;10(6):592.

[46]Ranganath AS, Ganesh VA, Sopiha K, Sahay R, Baji A. Thermoresponsive electrospun membrane with enhanced wettability. RSC advances 2017.89-19982:(32)7;

[47]Zou G, Shen J, Duan P, Xia X, Chen R, Jin B. Temperature-Sensitive Poly (N-isopropylacrylamide)/Konjac Glucomannan/Graphene Oxide Composite Membranes with Improved Mechanical Property, Swelling Capability, and Degradability. International Journal of Polymer Science 2018;2018.

[48]Wang H, Zhao Y, Wu Y, Hu Y-l, Nan K, Nie G, et al. Enhanced anti-tumor efficacy by co-delivery of doxorubicin and paclitaxel with amphiphilic methoxy PEG-PLGA copolymer nanoparticles. Biomaterials 2011;32.90-8281:(32)

[49]Ibrahim SM, El Salmawi KM, Zahran A. Synthesis of crosslinked superabsorbent carboxymethyl cellulose/acrylamide hydrogels through electron-beam irradiation. Journal of Applied Polymer Science 2007;104(3):2003-08.

[50]Zhang L, Guo R, Yang M, Jiang X, Liu B. Thermo and pH dual-responsive nanoparticles for anti-cancer drug delivery. Advanced Materials 2007;19(19):2988-92.

[51]Feng Y, Wang C, Ke F, Zang J, Zhu J. MIL-100 (Al) Gels as an Excellent Platform Loaded with Doxorubicin Hydrochloride for pH-Triggered Drug Release and Anticancer Effect. Nanomaterials 2018;8(6):446.

[52]Poudel AJ, He F, Huang L, Xiao L, Yang G. Supramolecular hydrogels based on poly (ethylene glycol)-poly (lactic acid) block copolymer micelles and α-cyclodextrin for potential injectable drug delivery system. Carbohydrate polymers 2018;194:69-79.

[53]Perera AS, Zhang S, Homer-Vanniasinkam S, Coppens M-O, Edirisinghe M. Polymer–magnetic composite fibers for remote-controlled drug release. ACS applied materials & interfaces 2.31-15524:(18)10;018

[54]Doppalapudi S, Jain A, Domb AJ, Khan W. Biodegradable polymers for targeted delivery of anti-cancer drugs. Expert opinion on drug delivery 2016;13(6):891-909.

[55]Li B, Xu H, Li Z, Yao M, Xie M, Shen H, et al. Bypassing multidrug resistance in human breast cancer cells with lipid/polymer particle assemblies. International journal of nanomedicine 2012;7:187.

[56]Ke W, Li J, Zhao K, Zha Z, Han Y, Wang Y, et al. Modular design and facile synthesis of enzyme-responsive peptide-linked block copolymers for efficient delivery of doxorubicin. Biomacromolecules 2016;17(10):3268-76.

[57]Galperin A, Long TJ, Garty S, Ratner BD. Synthesis and fabrication of a degradable poly (N-isopropyl acrylamide) scaffold for tissue engineering applications. Journal of Biomedical Materials Research Part A 2013;101(3):775-86.

[58]Lanzalaco S, Armelin E. Poly (n-isopropylacrylamide) and copolymers: A review on recent progresses in biomedical applications. Gels 2017;3(4):36.

[59]Brako F, Luo C, Craig DQ, Edirisinghe M. An Inexpensive, Portable Device for Point-of-Need Generation of Silver-Nanoparticle Doped Cellulose Acetate Nanofibers for Advanced Wound Dressing. Macromolecular Materials and Engineering 2018;303(5):1700586.

[60]Aydogdu MO, Altun E, Crabbe-Mann M, Brako F, Koc F, Ozen G, et al. Cellular interactions with bacterial cellulose: Polycaprolactone nanofibrous scaffolds produced by a portable electrohydrodynamic gun for point-of-need wound dressing. International wound journal 2018;15(5):789-97.